RSC Advances

PAPER

View Article Online
View Journal | View Issue

Cite this: *RSC Adv.*, 2024, **14**, 23459

Propane dehydrogenation catalysis of group IIIB and IVB metal hydrides†

Xiaoming Hu,[a] Mengwen Huang,[a] Tetsuya Kinjyo,[b] Shinya Mine,[c] Takashi Toyao,[a] Yoyo Hinuma,[d] Masaaki Kitano,[ef] Toyoto Sato,[g] Norikazu Namiki,[b] Ken-ichi Shimizu[a] and Zen Maeno*[b]

Received 1st April 2024
Accepted 6th July 2024

DOI: 10.1039/d4ra02473g

rsc.li/rsc-advances

Catalytic propane dehydrogenation (PDH) has mainly been studied using metal- and metal oxide-based catalysts. Studies on dehydrogenation catalysis by metal hydrides, however, have rarely been reported. In this study, PDH reactions using group IIIB and IVB metal hydride catalysts were investigated under relatively low-temperature conditions of 450 °C. Lanthanum hydride exhibited the lowest activation energy for dehydrogenation and the highest propylene yield. Based on kinetics studies, a comparison between the reported calculation results and isotope experiments, the hydrogen vacancies of metal hydrides were involved in low-temperature PDH reactions.

1. Introduction

Propane dehydrogenation (PDH) is a simple method used to synthesize propylene, which is an important bulk chemical for the production of polymers and other fine chemicals. Owing to the increasing demand for propylene brought about by the shift in feedstock from naphtha to shale gas, the development of PDH catalysts has recently attracted significant attention from academia and industry.[1–5] Commercially, PtSn alloys and CrO_X catalyst systems have been used for PDH.[6–9] Owing to the reaction's exothermic nature, the operating temperature was approximately 600 °C.[2] Significant efforts have been made toward developing metal- (mainly Pt and its alloy nanoparticles) and metal oxide-based (Ga_2O_3, Al_2O_3, TiO_2, ZrO_2, *etc.*) catalyst systems for efficient PDH reactions.[10–20] To develop new catalyst systems, the exploration of PDH catalysis by materials other than metals and metal oxides is of considerable interest.

Catalytic applications of hydrogen-containing compounds have been a topic of interest in catalysis research.[21–25] Several metal hydrides and hydrogen-containing mixed-anion compounds are effective catalysts and/or supports for the hydrogenation of CO_2 and N_2, with lattice hydrogen atoms and/or hydrogen vacancies playing an important role.[26–34] However, their effectiveness in dehydrogenation has not been reported since early studies were conducted in the 1920s–1950s.[35,36] Recently, our group reported that titanium hydrides exhibit a superior propylene formation rate compared to that achieved using titanium oxides at 450 °C.[37] As a continuation of that study, we investigated the PDH reaction over group IIIB (Sc, Y, and La) and IVB (Ti, Zr, and Hf) metal hydrides, all of which showed higher activity compared to that exhibited by the corresponding metal oxides at 450 °C. Among the tested metal hydrides, lanthanum hydride afforded the highest propylene yield. Notably, the activation barrier for PDH using lanthanum hydride was 34.6 kJ mol^{-1}, which is much lower than those using PtSn and CrO_X catalysts. The involvement of hydrogen vacancies in metal hydrides in low-temperature PDH reactions is also discussed.

2. Experimental

2.1. Catalyst preparation

The group IIIB metal hydrides (ScH_2, YH_3, and LaH_3) were prepared by reacting metal chips (purity: >99.9%, RARE METALLIC Co.,Ltd) in an H_2 atmosphere (1.5 MPa) at various temperatures (400 °C for ScH_2 and YH_3, room temperature for LaH_3) for 4 h. Other group IVB metal hydrides, ZrH_2 (powder, Mitsuwa Chemical Co.,Ltd) and HfH_2 (powder, <75 μm, purity: >99.5%, Goodfellow), were commercially obtained. The ball-milled metal hydrides were prepared using a Fritsch P-6

[a]*Institute for Catalysis, Hokkaido University, N-21, W-10, Sapporo 001-0021, Japan*
[b]*School of Advanced Engineering, Kogakuin University, 2665-1, Nakano-cho, Hachioji, 192-0015, Japan. E-mail: zmaeno@cc.kogakuin.ac.jp*
[c]*National Institute of Advanced Industrial Science and Technology (AIST), Research Institute for Chemical Process Technology, 4-2-1 Nigatake, Miyagino, Sendai 983-8551, Japan*
[d]*Department of Energy and Environment, National Institute of Advanced Industrial Science and Technology, 1-8-31, Midorigaoka, Ikeda 563-8577, Japan*
[e]*MDX Research Center for Element Strategy, International Research Frontiers Initiative, Tokyo Institute of Technology, Midori, Yokohama 226-8503, Japan*
[f]*Advanced Institute for Materials Research (WPI-AIMR), Tohoku University, Sendai 980-8577, Japan*
[g]*Department of Engineering Science and Mechanics, College of Engineering, Shibaura Institute of Technology, Tokyo 135-8548, Japan*

† Electronic supplementary information (ESI) available. See DOI: https://doi.org/10.1039/d4ra02473g

planetary ball mill. For example, LaH_3 (1 g) was milled together in an ZrO_2 pot (80 mL) with zirconia balls (ø5 mm, 100 g). The milling conditions were 200 rpm with a 1 min interval after every 6 min of milling for 1 h. In order to minimize the effect of oxidation on the experiment, the metal hydrides were handled in the glove box under an argon atmosphere. PtSn and CrO_X catalysts were prepared according to impregnation methods (The details are described in ESI†).

2.2. Catalytic reactions

Under an Ar atmosphere in a glove box, 100 mg of metal hydride was loaded into a U-shaped quartz reactor equipped with a 4-way valve. The reactor was removed, taking care to ensure no exposure to air, and placed in an electric furnace to conduct the PDH reaction (Fig. S1†). The propylene yield ($Y_{C_3H_6}$) was determined using a gas chromatograph equipped with a flame-ionizing detector (details are provided in ESI†). The compositions (C_n: n denotes the kind of gas) of methane, ethane, ethylene, propane, and propylene were determined on the basis of effective carbon numbers and GC areas. Note that other products with higher carbon number were not detected. The yield and selectivity of propylene were calculated from the gas compositions by the following equations.

$$\text{Conversion} = \frac{C_{C_3H_8\_in} - C_{C_3H_8}}{C_{C_3H_8\_in}}$$

$$\text{Yield} = \frac{C_{C_3H_6}}{\left(C_{CH_4} + C_{C_2H_6} + C_{C_2H_4} + C_{C_3H_6} + C_{C_3H_8}\right)}$$

$$\text{Selectivity} = \frac{C_{C_3H_6}}{\left(\frac{C_{CH_4}}{3} + \frac{2 \times C_{C_2H_4}}{3} + \frac{2 \times C_{C_2H_6}}{3} + C_{C_3H_6}\right)}$$

To investigate the temperature-dependency of formation rate, the PDH reaction was carried out under the following conditions: 100 mg of catalysts, 10 mL min^{-1} of 10% C_3H_8/He, 430–460 °C for metal hydrides, 410–440 °C for $PtSn/SiO_2$ and CrO_X–Al_2O_3. The average propylene formation rate at each temperature was used for data analysis. For the comparison among a series of metal hydrides, the propylene formation rate is calculated based on each mole of catalyst, while for the comparison of LaH_3 with PtSn and CrO_X catalysts, the propylene formation rate is calculated based on each gram of catalyst. For the effect of partial propane pressure, the reaction was performed under the following conditions: 100 mg of metal hydrides, 50 mL min^{-1} of 2–8% C_3H_8/He, 450 °C. For the effect of partial H_2 pressure, the reaction was performed under the following conditions: 100 mg of metal hydrides, 50 mL min^{-1} of 2–8% H_2 + 10% C_3H_8/He, 450 °C.

2.3. Temperature programmed desorption (TPD)

The TPD experiment was performed using 10 mg of as-prepared LaH_3 under He flow. The signal of hydrogen ($m/z = 2$) was observed by a quadrupole mass spectrometer (BELMASS, MicrotracBEL). After the signal for $m/z = 2$ was stable, the temperature was increased from 50 °C to 800 °C with ramping rate of 5 °C min^{-1}, then be kept for an hour.

2.4. Isotope experiment

100 mg of as-prepared LaH_3 or LaD_3 were used for PDH with monitoring the generated gases including H_2, HD ($m/z = 3$), and D_2 ($m/z = 4$), by BELMASS. LaD_3 was prepared from the La chip and D_2 in the similar way described above. To monitor the generated D_2, Ar was used as a carrier gas instead of He. The temperature was increased from room temperature to 450 °C in 20 minutes under Ar flow. After the signals for $m/z = 2$, 3, and 4 were stable, 10% C_3H_8/Ar was introduced at 450 °C to investigate PDH reactions.

3. Results and discussion

The PDH reactions using metal hydrides were carried out at 450 °C using a flow-type reactor under atmospheric pressure. The initial catalytic activities at 20 min were compared in Table 1. The group IIIB metal hydrides, such as ScH_2, YH_3, and LaH_3, exhibited higher $Y_{C_3H_6}$ values (0.3–0.5%) than group IVB metal hydrides such as TiH_2, ZrH_2, and HfH_2 (0.1–0.2%). To increase $Y_{C_3H_6}$, a series of metal hydrides were ball milled (BM) to increase surface area. The specific surface area values, as determined by N_2 adsorption, increased from <1.0 to 4.2–12.5 $m^2 g^{-1}$, resulting in improved $Y_{C_3H_6}$ values from 0.1–0.5% to 1.2–11.0%, with LaH_3_BM presenting the highest $Y_{C_3H_6}$ (Fig. 1). The propylene formation rate normalized specific surface area of ball-milled LaH_3 was also highest. The ball-milled LaH_3, TiH_2,

Table 1 PDH reactions using group IIIB and IVB metal hydrides/oxides at 450 °C

Catalyst	Conv.[a] (%)	$S_{C_3H_6}$[a] (%)	$Y_{C_3H_6}$[a] (%)
ScH_2	0.5	>99.9	0.5
ScH_2_BM	8.3	36.6	3.1
Sc_2O_3	0.1	17.6	<0.1
YH_3	0.5	60.4	0.3
YH_3_BM	4.5	53.2	2.4
Y_2O_3	<0.1	58.7	<0.1
LaH_3	0.6	88.8	0.5
LaH_3_BM	11.8	92.7	11.0
La_2O_3	0.4	34.8	0.1
TiH_2	0.4	52.6	0.2
TiH_2_BM	1.5	82.6	1.2
TiO_2_Anatase	0.5	73.0	0.4
TiO_2_Rutile	0.7	96.1	0.7
ZrH_2	0.2	90.5	0.2
ZrH_2_BM	1.9	86.6	1.7
ZrO_2	0.4	47.7	0.2
HfH_2	0.2	82.9	0.2
HfH_2_BM	2.5	81.8	2.0
HfO_2	0.0	56.2	0.0

[a] Reaction conditions: 100 mg of catalyst, 10 mL min^{-1} of 10% C_3H_8/He, and 450 °C. Details of determination are described in Experimental section.

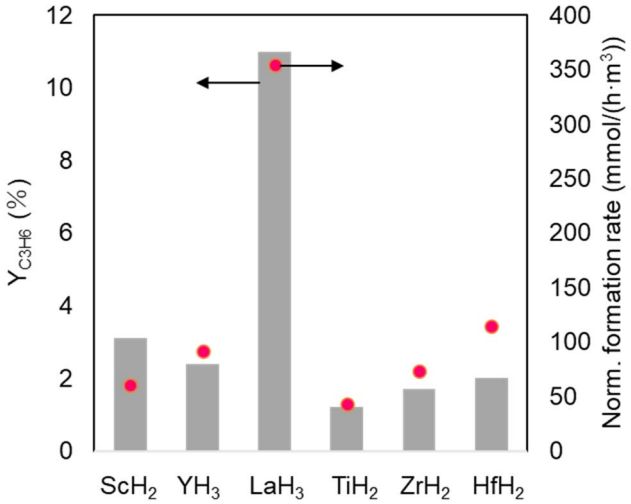

Fig. 1 $Y_{C_3H_6}$ and normalized formation rate based on surface area in PDH using group IIIB and IVB metal hydrides (ball-milled for 1 h) at 450 °C.

ZrH_2, and HfH_2 showed relatively good propylene selectivity ($S_{C_3H_6}$) (81.8–92.7%), whereas the ball-milled ScH_2 and YH_3 showed moderate to low $S_{C_3H_6}$ of 36.6% and 53.2%, respectively. The main byproduct was methane regardless of different metal hydrides. The possible reason for decrease of $S_{C_3H_6}$ is the cracking reaction of propane with hydrides derived from metal hydride catalysts. To discuss this possibility, we investigated H_2 TPD experiments for ScH_2 (as-prepared) and ScH_2_BM because the biggest decrease of $S_{C_3H_6}$ from 99.9% to 36.6% was observed. The H_2 desorption occurred above 500 °C for as-prepared ScH_2 (Fig. S2†). In contrast, the main desorption peaks shifted to lower temperature region (below 500 °C), supporting the above hypothesis. The favorable $S_{C_3H_6}$ of LaH_3_BM was maintained by extending the reaction time from 20 to 120 min, although the $Y_{C_3H_6}$ unfortunately decreased (Fig. S3 and S4†). PDH catalysis using group IIIB and IVB metal oxides was investigated under similar reaction conditions because some of them, such as TiO_2 and ZrO_2, have been reported to exhibit considerable activity for alkane dehydrogenation.[15,16] Each metal oxide demonstrated a lower $Y_{C_3H_6}$ and propylene formation rate (normalized based on the specific surface area value) than those of the corresponding metal hydrides, proving that group IIIB and IVB metal hydrides have the potential to be effective catalysts for low-temperature PDH reactions.

Our previous study on PDH over TiH_2 revealed that partially dehydrogenated titanium hydrides are more active than Ti metal.[37] In this study, LaH_3 was pre-treated under He flow at different temperatures to promote the desorption of lattice hydrogen and was then applied to the PDH reaction at 450 °C. The He treatments at 450 and 600 °C did not significantly affect the reaction, and thus similar $Y_{C_3H_6}$ values were obtained (0.5%, Fig. 2a). When the pre-treatment temperature was increased to 700 and 800 °C, $Y_{C_3H_6}$ decreased to 0.3% and <0.1%, respectively. In the TPD of LaH_3, a small desorption peak at 300–500 °C and a larger peak at 700–800 °C were observed (Fig. 2b). The loss of activity by high temperature pretreatment is possibly deep dehydrogenation of LaH_3 to La metal. To discuss this consideration, we conducted H_2 TPD of LaH_3 up to 800 °C to completely release hydrides and then successively investigated H_2 temperature programmed reduction (TPR) to study the H_2 absorption property. The main H_2 absorption peak was observed from 300–400 °C (Fig. S5†). The H_2-treated sample showed the intermediate $Y_{C_3H_6}$ value (0.3%), which was lower than that of fresh LaH_3 (0.5%) and higher than Ar-treated one (<0.1%), supporting the above consideration.

The XRD measurements of LaH_3 before and after PDH at 450 °C showed that the diffraction peaks shifted toward lower angles after the reaction (Fig. S6†). A decrease in hydrogen content induces lattice expansion in the lanthanum hydride system.[38] To study the change of lattice constant in detail, the synthesized LaH_3 was treated under argon or propane (1 atm) atmosphere at 450 °C in a batch reactor, and then the treated samples were characterized by XRD with using Si powder as an internal standard (Fig. 3a and b). Using indexing program TREOR97 and least-squares refinement of lattice constant program PIRUM (see ESI†), observed Bragg peaks of as-prepared sample were indexed by a pseudo-cubic unit cell with a = 5.6119(11) Å, which corresponds to H/La = 2.77 as estimated by comparison with calculated lattice constant of LaH_3 and LaH_2 (Fig. 3c), showing the formation of relatively highly-hydrogenated lanthanum hydrides. The treatment under argon (as an inert gas) induced the increase of lattice constant to 5.6188(8) Å (the pseudo-cubic unit cell), and the propane treatment resulted in the further slightly increase to 5.6246(4) Å (the pseudo-cubic unit cell). The estimated H/La values were 2.61 and 2.49, respectively. These results show that the formation of hydrogen vacancy mainly occurred by thermal treatment and indicate that the incorporation of hydrogen derived from propane into the generated vacancy is unlikely to occur during PDH.

We also investigated the PDH using LaH_3 under higher space velocity conditions (100 mL min^{-1} of 10% C_3H_8/Ar). The detailed results including the carbon balance value were shown in Table S1.† Although the initial conversion was relatively high (15.4%), the $S_{C_3H_6}$ value was quite low owing to cracking reaction and the carbon balance was moderate (60%), resulting in a low $Y_{C_3H_6}$. The conversion decreased to 2–3% whereas was good $S_{C_3H_6}$ and carbon balance values was maintained. The used catalyst was treated with H_2 at 300 °C to try to regenerate the initial activity. Unfortunately, the initial activity was not recovered (Table S2†), indicating that deep dehydrogenation is unlikely to cause the deactivation. The specific surface area of the used ball-milled LaH_3 was 6.5 m^2 g^{-1}, which was similar to the original one (7.5 m^2 g^{-1}), indicating that the sintering was unlikely to occur. Because the carbon balance value at initial stage was relatively low in PDH using fresh LaH_3, the coke formation is more plausible reason for deactivation.

The temperature dependence of the propylene formation rate using different metal hydrides was plotted, and the apparent activation energies (E_a) were compared. TiH_2 was excluded because the E_a value is too dependent on H_2 co-feeding due to the interconversion between titanium hydride

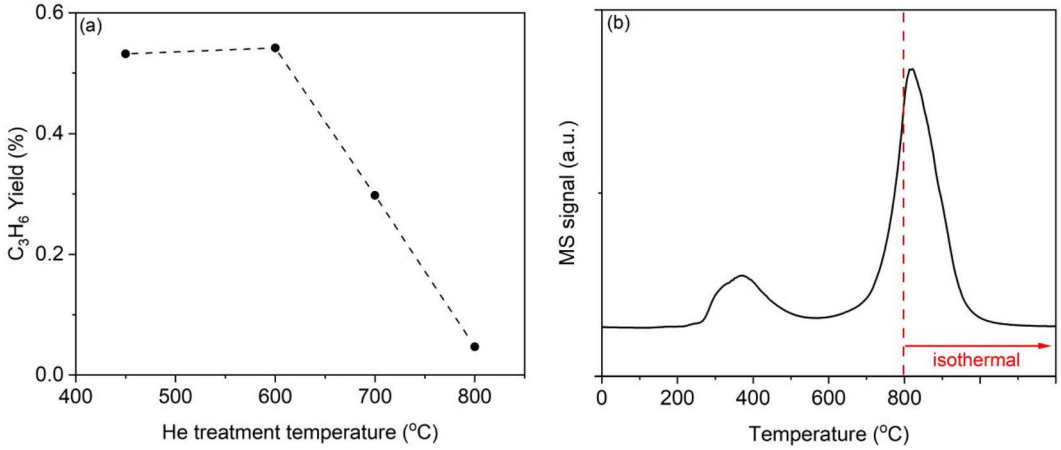

Fig. 2 (a) $Y_{C_3H_6}$ in PDH using LaH_3 pre-treated under He flow at different temperatures. LaH_3 was used as a catalyst, and the PDH reaction was performed at 450 °C. (b) H_2 TPD profile of the LaH_3 under He flow ($m/z = 2$).

and Ti metal.[37] The E_a values for the group IIB metal hydrides were lower than those for the group IVB metal hydrides (Fig. 4a). LaH_3 exhibited the lowest E_a (34.6 kJ mol^{-1}), whereas the highest E_a (147.5 kJ mol^{-1}) was observed for HfH_2. Notably, under low-temperature conditions, the E_a for LaH_3 is lower than those for PtSn- and CrO_x-based catalysts (74.0 and 94.0 kJ mol^{-1}, respectively), as shown in Fig. 4b. In addition, industrially used K–PtSn/Al_2O_3 was prepared according to the previous report and investigated kinetic study. The E_a value (117 kJ mol^{-1}) was higher than that for LaH_3 (Fig. S7†), indicating the high catalytic potential of LaH_3.

In previous studies on PDH over group IVB metal oxides, such as TiO_2 and ZrO_2, oxygen vacancies generated by H_2 or CO pre-treatment were involved in C–H bond cleavage, promoting PDH.[15,16] In this study, we discuss the possible involvement of hydrogen vacancies during PDH based on partial pressure changes and the relationship between activity and the formation energy of surface hydrogen vacancies. The effects of the partial pressures of propane and H_2 ($p(C_3H_8)$ and $p(H_2)$) on PDH using LaH_3 were investigated. The reaction order of $p(H_2)$ was determined to be approximately −0.5, whereas the reaction order of $p(C_3H_8)$ was relatively low and positive (approx. 0.2) (Fig. 5). Similar partial pressure effects were observed in the PDH using another metal hydride (Fig. S8†). Interestingly, the PtSn-based catalyst system exhibited a zero-order dependency on $p(H_2)$.[39,40] It can be considered that an increase in $p(H_2)$ suppresses the formation of hydrogen vacancies, resulting in a decreased propylene formation rate. The initial $Y_{C_3H_6}$ values are plotted as a function of theoretical formation energies of the surface hydrogen vacancies ($E_{H_{vac}}$).[41] As $E_{H_{vac}}$ decreased, the initial $Y_{C_3H_6}$ increased, and the lanthanum hydrides possessing the lowest $E_{H_{vac}}$ exhibited the highest $Y_{C_3H_6}$ (Fig. 6). These results imply that hydrogen vacancies in metal hydrides are involved in the PDH reaction.

To further investigate the involvement of hydrogen vacancies, LaD_3 was prepared from a lanthanum chip and D_2 gas for testing in the PDH reaction. The generated gas products, including H_2, HD, and D_2, were monitored using mass spectrometry ($m/z = 2$, 3, and 4, respectively) and then compared with the PDH reactions using LaH_3. During the pre-treatment of LaH_3 under Ar flow, H_2 desorption occurred as the temperature was increased from room temperature to 450 °C (Fig. S9†),

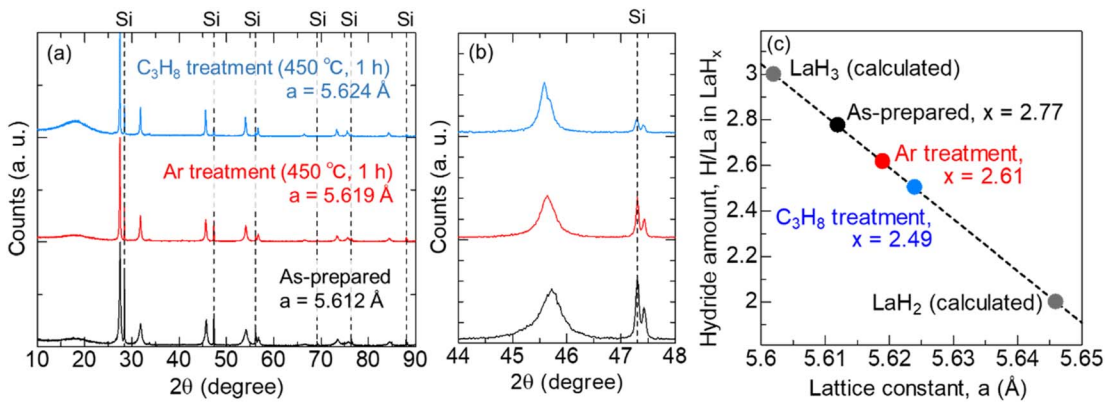

Fig. 3 XRD measurement of as-prepared, Ar-treated, and C_3H_8-treated LaH_3 using Si as an internal standard. (a) Full-range XRD pattern and (b) enlarged view. (c) Estimated hydrogen amount (H/La) based on lattice constant.

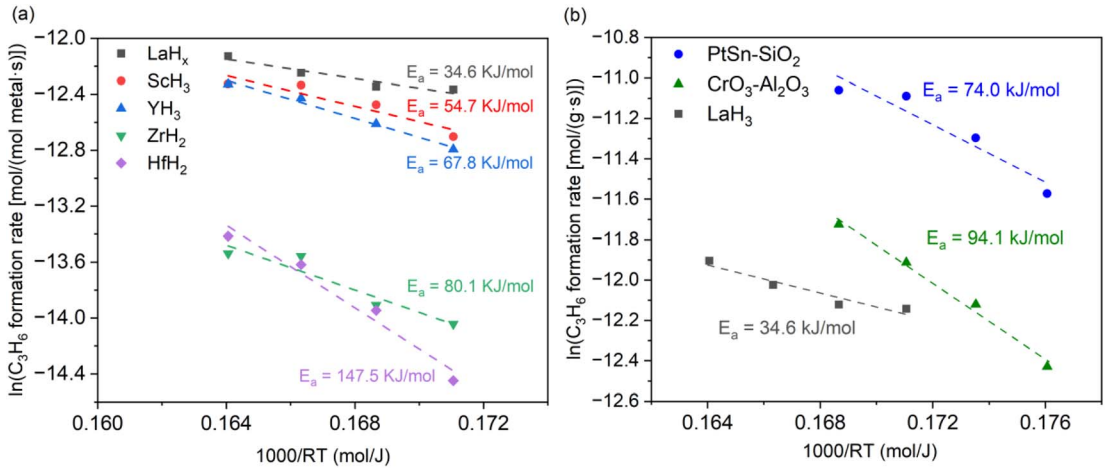

Fig. 4 Temperature dependence of propylene formation rate in PDH using (a) a series of metal hydrides and (b) PtSn- and CrO_X-based catalysts.

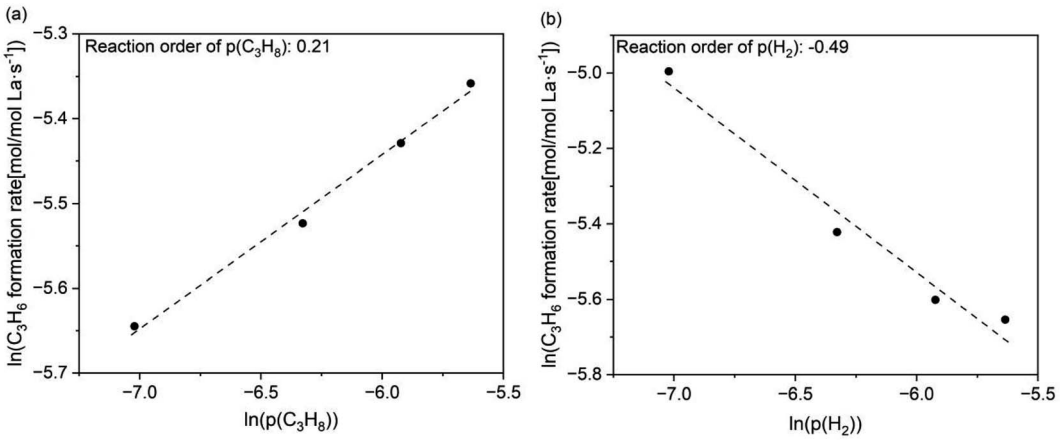

Fig. 5 Effects of the partial pressures of C_3H_8 and H_2 ($p(C_3H_8)$ and $p(H_2)$) on PDH using LaH_3. (a) Effect of $p(C_3H_8)$ (C_3H_8 concentration: 2–8%, without H_2 co-feeding). (b) Effect of $p(H_2)$ (C_3H_8 concentration: 10% (fixed), H_2 concentration: 2–8%). 100 mg of LaH_3 was used, and the total flow rate was fixed at 50 mL min^{-1}.

indicating the generation of hydrogen vacancies under PDH reaction conditions. After the introduction of propane at 450 °C, H_2 was formed, and D_2 and HD were barely detected (Fig. 7a). When LaD_3 was used instead of LaH_3, D_2 desorption was observed during a similar pre-treatment under Ar flow (Fig. S9†). In the PDH reaction, D_2 and HD were simultaneously formed, and the signal intensity for H_2 was much lower than that observed when using LaH_3 (Fig. 7b). In a separate experiment, LaD_3 exhibited PDH activity, in which the time course of $Y_{C_3H_6}$ was similar to that obtained when using LaH_3 (Fig. S10†). These results indicate that the H atoms of C_3H_8 are incorporated into the hydrogen vacancies of LaD_3 and then exchanged/combined with lattice D atoms, resulting in the formation of D_2/HD as co-products. To determine whether an exchange reaction occurred between LaD_3 and the gas-phase H_2, the H–D exchange reaction of LaD_3 with H_2 was also conducted at 450 °C. The peak for D_2 immediately appeared after Ar pre-treatment and the introduction of H_2, while the signals for HD and H_2 were hardly detected directly after the introduction of H_2. With

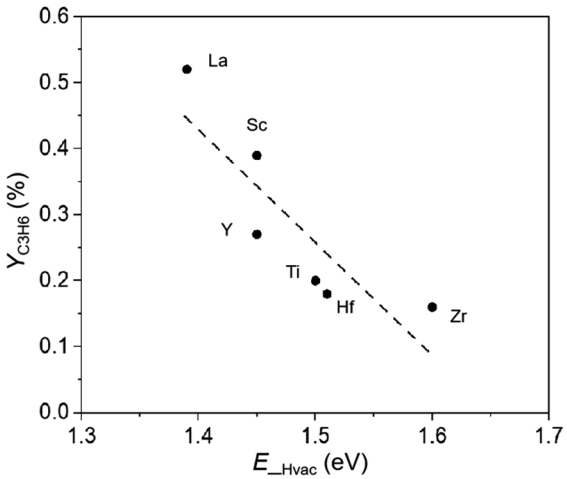

Fig. 6 Correlation of initial $Y_{C_3H_6}$ with theoretical formation energy of surface hydrogen vacancies ($E_{-H_{vac}}$) for group IIIB and IVB metal hydrides.[41]

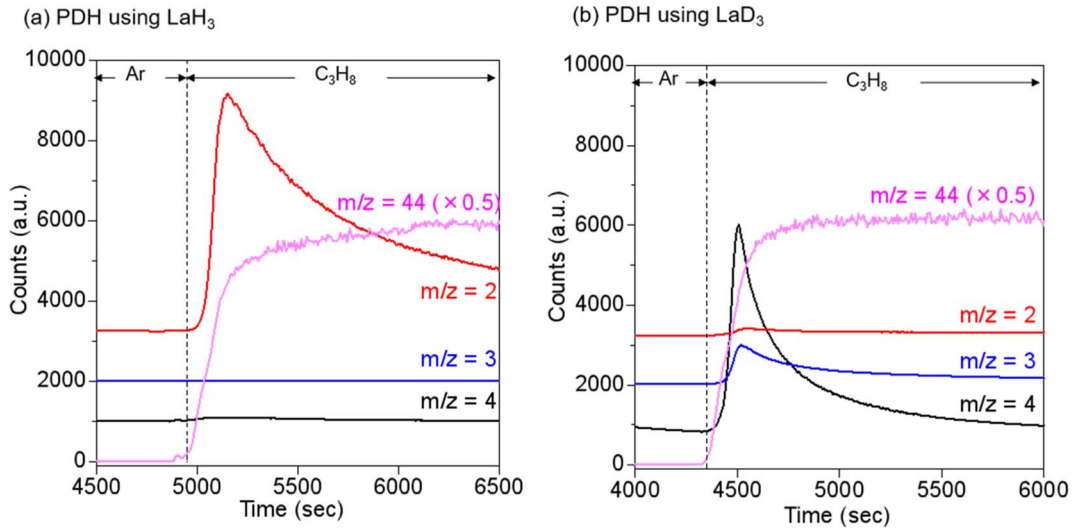

Fig. 7 Gas products in PDH using (a) LaH_3 and (b) LaD_3 as monitored by mass spectrometry. The reaction temperature was isothermal after being increased from 30 to 450 °C. After the signals for H_2 or D_2 stabilized, propane was introduced at a concentration of 10%. The total flow rate was 10 mL min^{-1}, and the carrier gas was Ar. The mass numbers of the gases shown are m/z = 2 (H_2), 3 (HD), 4 (D_2), and 44 (C_3H_8).

a decreasing signal for D_2, a peak for HD formation was observed, and the signal intensity for H_2 increased (Fig. S11†). This observation was different from that of the PDH reaction, suggesting that the exchange reaction of LaD_3 with H_2 was not a plausible formation pathway for D_2 or HD. These isotope experiments provide further indicate for the involvement of the hydrogen vacancies in LaH_3 in PDH reactions.

4. Conclusions

In conclusion, the low-temperature activities of group IIIB and IVB metal hydrides in PDH reactions were investigated. All the metal hydrides exhibited higher activity than the corresponding metal oxides. Among the tested metal hydrides, LaH_3 was the most active and reacted through the lowest activation barrier, which was significantly lower than those observed for PtSn- and CrO_X-based catalyst systems. Kinetics studies and isotope experiments indicated that hydrogen vacancies are possibly involved in low-temperature PDH using metal hydrides. Although the durability and reusability of La hydrides are relatively low as PDH catalysts, our findings demonstrate the potential of bulk metal hydrides to activate light alkanes under non-oxidative conditions.

Data availability

The data that support the findings of this study are available from the corresponding author, Z. M., upon reasonable request.

Author contributions

Z. M. conceived the idea of study and supervised the conduct of this study. X. H., M. H., and S. M. performed the experiments for catalyst preparation and catalytic reactions. Y. H. analyzed the experimental data based on computational study. M. K. synthesized a part of metal hydrides. T. K. and T. S. conducted the XRD measurements and details analysis. X. M. also wrote the draft, and T. T., N. N. K. S., and Z. M. critically reviewed it. All authors approved the final version of the manuscript to be published.

Conflicts of interest

The authors declare no competing financial interest.

Acknowledgements

This study was financially supported by KAKENHI (Grant No. JP20H02518, JP20H02775, JP20KK0111, and JP21H04626) from the Japan Society for the Promotion of Science (JSPS) and KAKENHI on Innovative Areas "Hydrogenomics" (No. JP21H00019 and JP21H00012). This study was also supported by the JST-CREST project JPMJCR17J3, JST-SPRING project JPMJSP2119, and Joint Usage/Research Center for Catalysis.

References

1 S. Chen, X. Chang, G. Sun, T. Zhang, Y. Xu, Y. Wang, C. Pei and J. Gong, *Chem. Soc. Rev.*, 2021, **50**, 3315–3354.
2 J. J. H. B. Sattler, J. Ruiz-Martinez, E. Santillan-Jimenez and B. M. Weckhuysen, *Chem. Rev.*, 2014, **114**, 10613–10653.
3 O. O. James, S. Mandal, N. Alele, B. Chowdhury and S. Maity, *Fuel Process. Technol.*, 2016, **149**, 239–255.
4 M. Artetxe, G. Lopez, M. Amutio, G. Elordi, J. Bilbao and M. Olazar, *Chem. Eng. J.*, 2012, **207–208**, 27–34.
5 A. Corma, F. V. Melo, L. Sauvanaud and F. Ortega, *Catal. Today*, 2005, **107–108**, 699–706.
6 J. Wang, Y. H. Song, Z. T. Liu and Z. W. Liu, *Appl. Catal., B*, 2021, **297**, 120400.

7 L. Liu, M. Lopez-Haro, C. W. Lopes, S. Rojas-Buzo, P. Concepcion, R. Manzorro, L. Simonelli, A. Sattler, P. Serna, J. J. Calvino and A. Corma, *Nat. Catal.*, 2020, **3**, 628–638.
8 Z. P. Hu, Y. Wang, D. Yang and Z. Y. Yuan, *J. Energy Chem.*, 2020, **47**, 225–233.
9 Y. Shan, Z. Sui, Y. Zhu, D. Chen and X. Zhou, *Chem. Eng. J.*, 2015, **278**, 240–248.
10 B. Zheng, W. Hua, Y. Yue and Z. Gao, *J. Catal.*, 2005, **232**, 143–151.
11 Y. Xie, W. Hua, Y. Yue and Z. Gao, *Chin. J. Chem.*, 2010, **28**, 1559–1564.
12 T. P. Otroshchenko, V. A. Kondratenko, U. Rodemerck, D. Linke and E. V. Kondratenko, *Catal. Sci. Technol.*, 2017, **7**, 4499–4510.
13 D. Shee and A. Sayari, *Appl. Catal., A*, 2010, **389**, 155–164.
14 E. V. Kondratenko, *J. Catal.*, 2017, **348**, 282–290.
15 Y. Zhang, Y. Zhao, T. Otroshchenko, H. Lund, M. M. Pohl, U. Rodemerck, D. Linke, H. Jiao, G. Jiang and E. V. Kondratenko, *Nat. Commun.*, 2018, **9**, 3794.
16 C. F. Li, X. Guo, Q. H. Shang, X. Yan, C. Ren, W. Z. Lang and Y. J. Guo, *Ind. Eng. Chem. Res.*, 2020, **59**, 4377–4387.
17 Y. Nakaya and S. Furukawa, *ChemPlusChem*, 2022, **87**, e202100560.
18 L. Rochlitz, Q. Pessemesse, J. W. A. Fischer, D. Klose, A. H. Clark, M. Plodinec, G. Jeschke, P. A. Payard and C. Copéret, *J. Am. Chem. Soc.*, 2022, **144**, 13384–13393.
19 M. D. Marcinkowski, M. T. Darby, J. Liu, J. M. Wimble, F. R. Lucci, S. Lee, A. Michaelides, M. Flytzani-Stephanopoulos, M. Stamatakis and E. C. H. Sykes, *Nat. Chem.*, 2018, **10**, 325–332.
20 H. Zhang, Y. Jiang, G. Wang, N. Tang, X. Zhu, C. Li and H. Shan, *Mol. Catal.*, 2022, **519**, 112143.
21 H. Hosono and M. Kitano, *Chem. Rev.*, 2021, **121**, 3121–3185.
22 H. Nishino, T. Fujita, N. T. Cuong, S. Tominaka, M. Miyauchi, S. Iimura, A. Hirata, N. Umezawa, S. Okada, E. Nishibori, A. Fujino, T. Fujimori, S. I. Ito, J. Nakamura, H. Hosono and T. Kondo, *J. Am. Chem. Soc.*, 2017, **139**, 13761–13769.
23 K. Hayashi, P. V. Sushko, Y. Hashimoto, A. L. Shluger and H. Hosono, *Nat. Commun.*, 2014, **5**, 3515.
24 K. Fukutani, J. Yoshinobu, M. Yamauchi, T. Shima and S. Orimo, *Catal. Lett.*, 2022, **152**, 1583–1597.
25 H. Kageyama, K. Hayashi, K. Maeda, J. P. Attfield, Z. Hiroi, J. M. Rondinelli and K. R. Poeppelmeier, *Nat. Commun.*, 2018, **9**, 772.
26 Y. Tsuji, K. Okazawa, Y. Kobayashi, H. Kageyama and K. Yoshizawa, *J. Phys. Chem. C*, 2021, **125**, 3948–3960.
27 S. Kato, S. K. Matam, P. Kerger, L. Bernard, C. Battaglia, D. Vogel, M. Rohwerder and A. Züttel, *Angew. Chem., Int. Ed.*, 2016, **55**, 6028–6032.
28 Y. Cao, A. Saito, Y. Kobayashi, H. Ubukata, Y. Tang and H. Kageyama, *ChemCatChem*, 2021, **13**, 191–195.
29 M. Miyazaki, K. Ogasawara, T. Nakao, M. Sasase, M. Kitano and H. Hosono, *J. Am. Chem. Soc.*, 2022, **144**, 6453–6464.
30 Y. Kobayashi, Y. Tang, T. Kageyama, H. Yamashita, N. Masuda, S. Hosokawa and H. Kageyama, *J. Am. Chem. Soc.*, 2017, **139**, 18240–18246.
31 M. Kitano, J. Kujirai, K. Ogasawara, S. Matsuishi, T. Tada, H. Abe, Y. Niwa and H. Hosono, *J. Am. Chem. Soc.*, 2019, **141**, 20344–20353.
32 P. Wang, F. Chang, W. Gao, J. Guo, G. Wu, T. He and P. Chen, *Nat. Chem.*, 2017, **9**, 64–70.
33 M. Hattori, S. Iijima, T. Nakao, H. Hosono and M. Hara, *Nat. Commun.*, 2020, **11**, 2001.
34 C. Färber, P. Stegner, U. Zenneck, C. Knüpfer, G. Bendt, S. Schulz and S. Harder, *Nat. Commun.*, 2022, **13**, 3210.
35 L. Wright and S. Weller, *J. Am. Chem. Soc.*, 1954, **76**, 5305–5308.
36 V. V. Lunin, G. V. Lisichkin, Y. V. Vlasenko and A. E. Agronomov, *Zh. Fiz. Khim.*, 1974, **48**, 2465.
37 S. Yasumura, Y. Wen, T. Toyao, Y. Kanda, K. Shimizu and Z. Maeno, *Chem. Lett.*, 2022, **51**, 88–90.
38 P. Klavins, R. N. Shelton, R. G. Barnes and B. J. Beaudry, *Phys. Rev. B: Condens. Matter Mater. Phys.*, 1984, **29**, 5349.
39 S. Saerens, M. K. Sabbe, V. V. Galvita, E. A. Redekop, M. F. Reyniers and G. B. Marin, *ACS Catal.*, 2017, **7**, 7495–7508.
40 G. di Wang, J. W. Jiang, Z. J. Sui, Y. A. Zhu and X. G. Zhou, *ACS Omega*, 2022, **7**, 30773–30781.
41 Y. Hinuma, S. Mine, T. Toyao, Z. Maeno and K. Shimizu, *Phys. Chem. Chem. Phys.*, 2021, **23**, 16577–16593.